

PCCP

Accepted Manuscript



This is an *Accepted Manuscript*, which has been through the Royal Society of Chemistry peer review process and has been accepted for publication.

Accepted Manuscripts are published online shortly after acceptance, before technical editing, formatting and proof reading. Using this free service, authors can make their results available to the community, in citable form, before we publish the edited article. We will replace this *Accepted Manuscript* with the edited and formatted *Advance Article* as soon as it is available.

You can find more information about *Accepted Manuscripts* in the [Information for Authors](#).

Please note that technical editing may introduce minor changes to the text and/or graphics, which may alter content. The journal's standard [Terms & Conditions](#) and the [Ethical guidelines](#) still apply. In no event shall the Royal Society of Chemistry be held responsible for any errors or omissions in this *Accepted Manuscript* or any consequences arising from the use of any information it contains.

Dielectric and Raman investigations of structural phase transitions in $(\text{C}_2\text{H}_5\text{NH}_3)_2\text{CdCl}_4$

Ruchika Yadav^{‡a}, Diptikanta Swain^b, Partha P. Kundu^{b,c}, Harikrishnan S. Nair^{d,e}, Chandrabhas Narayana^b and Suja Elizabeth^a

Temperature-dependent Raman and dielectric measurements have been carried out on $(\text{C}_2\text{H}_5\text{NH}_3)_2\text{CdCl}_4$ single crystals. Raman studies reveal presence of two structural phase transitions below room temperature at 216 K and 114 K. The phase transitions are marked by anomalies in temperature dependence of wave-number and full width half maximum (FWHM) of several vibrational modes. The transitions are also accompanied by anomalies in dielectric measurements. Raman and dielectric data indicate that the transition at 216 K is order-disorder in nature and is driven by re-orientation of organic ions, while transition at 114 K is due to coupling between the CdCl_6 octahedron and organic chain. Further high temperature dielectric measurements reveal presence of one more structural phase transition around 473 K across which dispersion in dielectric parameters is observed. Activation energies and relaxation time obtained for high temperature dielectric phases are characteristic of combined reorientation motions of alkyl ammonium cations.

1 Introduction

Hybrid organic-inorganic perovskite materials are few of the most extensively studied crystalline hybrid compounds, by virtue of their multifunctional behaviour and potential applications^{1–7}. They consist of a wide range of inorganic anion chains (an extended network of corner-sharing metal oxide or halide complexes), alternating with large variety of organic cations as building blocks. The organic component of the hybrid complex provides several useful properties such as structural flexibility, optical properties, etc, while the inorganic part is responsible for mechanical and thermal stability, interesting magnetic and dielectric transitions, etc^{4,8–10}. We can combine the useful properties of organic and inorganic components at single molecular level to tailor new multifunctional materials. Few such examples are $[(\text{CH}_3)_2\text{NH}_2]\text{Mn}(\text{HCOO})_3$ ^{11,12} and $[\text{NH}_4]\text{Mn}(\text{HCOO})_3$ ¹³, metal organic frameworks with perovskite structure. Both materials show transitions from a disordered state to an ordered state at low temperature as a result of hydrogen bonding between organic and inorganic components. $[(\text{CH}_3)_2\text{NH}_2]\text{Mn}(\text{HCOO})_3$ ¹¹ undergoes paraelectric to antiferroelectric transition at 185 K, while $[\text{NH}_4]\text{Mn}(\text{HCOO})_3$ ¹³ transforms to ferroelectric phase below 250 K, both being accompanied by structural transition. The compounds show

weak ferromagnetism at temperatures below 10 K. This demonstrates that the organic and inorganic parts can be chosen and optimized to allow compositions with desirable multifunctional characteristics.

In this respect, crystals of metal ion complex with organic molecules are worth revisiting. Of particular interest were crystals of alkyl ammonium metal halides $(\text{C}_n\text{H}_{2n+1}\text{NH}_3)_2\text{MCl}_4$ ($\text{M} = \text{Mn}, \text{Cu}, \text{Cd}, \text{Fe}$). These belong to a family of ABX_3 perovskite consisting of nearly isolated layers of corner-sharing MCl_6 octahedrons sandwiched by alkyl-ammonium cations $(\text{C}_n\text{H}_{2n+1}\text{NH}_3)^+$ abbreviated as MA (methyl-ammonium) for $n = 1$ and EA (ethyl-ammonium) for $n = 2$ ^{14–16}. Ammonium group of the alkyl ammonium cations are present in the cavities between $\text{M}-\text{Cl}$ octahedron, and forms $\text{N}-\text{H}\cdots\text{Cl}$ hydrogen bonds with them. Adjacent layers are stacked upon each other through Vander Waal force between the terminal methyl groups. Additionally coulomb interactions are also present between transition metal ions (negatively charged octahedron) and organic cations. The interaction between two layers is much weaker compared to intra-layer interactions.

These compounds usually self-assemble at ambient temperature from solutions and are stable up to 200 °C. They display a variety of physical properties depending on the transition metal cation. For Cu, the system exhibits multiferroic behaviour where ferroelectric ordering is observed below 250 K and magnetic spins align antiferromagnetically below 8 K¹⁷. A non-magnetic semi-conducting nature is observed for Pb while the Cd and Zn analogues show insulating behaviour¹⁸. The crystal structure varies with temperature and pressure^{19–21}. All compounds of this series show orthorhombic structure at room temperature and undergo a series of structural changes due to different arrangements of alkyl ammonium chains. The choice of hydrogen bonding scheme is important in determining the orientation of organic molecule, thereby influencing the structural

^{0a} Department of Physics, Indian Institute of Science, Bangalore-560012, India; E-mail: ruchika@physics.iisc.ernet.in

^{0b} Chemistry and Physics of Materials Unit, Jawaharlal Nehru Centre for Advanced Scientific Research, Jakkur, P.O. Bangalore 560064, India.

^{0c} Department of Physics, M.S. Ramaiah University of Applied Sciences, Bangalore-560058, India.

^{0d} Highly Correlated Matter Research Group, Physics Department, P. O. Box 524, University of Johannesburg, Auckland Park 2006, South Africa.

^{0e} JCNS 2/Peter Grünberg Institute 4, Forschungszentrum Jülich, 52425 Jülich, Germany.

^{0‡} Corresponding Author.

phase transition²². Cd and Mn analogues, represent pseudo tetragonal lattice, and the system goes to tetragonal symmetry by a small shift in mean positions of atoms. At higher temperature, the compounds display orthorhombic to tetragonal structural transition at 394 K for $M=Mn^{2+}$ and 484 K for $M=Cd^{2+}$ respectively²¹. Two more structural transitions are observed at low temperatures (at 114 K and 216 K for $M=Cd$)^{21,23}. In the present investigation, we have analysed the mechanism of phase transitions in $(C_2H_5NH_3)_2CdCl_4$ using temperature dependent dielectric studies and Raman spectroscopy. Dielectric measurements provide insight into transport mechanism across the transition, at the same time Raman spectroscopy captures the dynamics and local structural changes with temperature.

2 Experimental

Single crystals of $(C_2H_5NH_3)_2CdCl_4$ (EA- $CdCl_4$) were grown by slow evaporation from aqueous solution containing stoichiometric amounts of precursors, as described elsewhere²⁴. The quality of the crystals used for experiments was checked under polarizing microscope. For dielectric measurements silver electrodes were deposited on oriented samples. All temperature and frequency dependent dielectric measurements were carried out in the temperature range 50 to 300 K, in a Closed Cycle Refrigerator using Agilent 4294 A Precision Impedance Analyser. The temperature evolution of Raman Spectra of $(C_2H_5NH_3)_2CdCl_4$ was recorded in the 180° backscattering geometry using 532 nm excitation from a diode pumped frequency doubled Nd:YAG solid state laser (model GDLM-5015 L, Photop Suwtech Inc., China) and a custom-built Raman spectrometer equipped with a spex triax 550 monochromator and a liquid nitrogen CCD (spectrum one with CCD 3000 controller, ISA Jobin Yovn)²⁵. Laser power on the sample was about 6 mW, and a typical spectral acquisition time of 4 min was used with spectral resolution of 2 cm^{-1} . The temperature was controlled with an accuracy of (± 0.1) K with the help of a temperature controller equipped with cooling stage (Linkam THMS 600). The spectral profile was fitted using a Lorentzian function with the appropriate background.

All density functional theory (DFT) calculations were performed by Gaussian 09 program²⁶ and geometrical optimization was carried out using hybrid exchange-correlation functional Becke3LeeYangParr (B3LYP)^{27,28}. Basis sets of C, H, N and Cl atoms were chosen 6-31G(d) and the valence and inner shell electrons of Cd atoms were described by basis set LANL2DZ and corresponding relativistic effective core potential respectively²⁹. In order to mimic the solid environment 12 organic components and 2 $CdCl_2$ units were chosen as shown in Fig 1. The organic units at the corners were frozen in order to prevent the structure from collapse in the gas phase since the charges in each fragments are opposite in polarity. The

harmonic Raman frequencies were computed on the optimized structures using the same level. Since the theoretical approach and basis set is incomplete, and an-harmonicity is neglected, the experimental data and theoretically calculated values were matched with a scaling factor of 0.961³⁰ for frequencies above 1000 cm^{-1} .

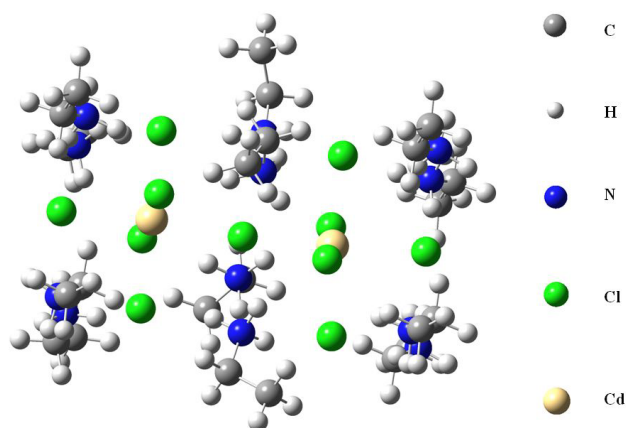


Figure 1 Structure of $(C_2H_5NH_3)_2CdCl_4$ used for calculating raman modes using Gaussian software.

3 Results and Discussions

3.1 Dielectric measurements

Presence of organic molecules with dipoles and the two-dimensional structure of $EA-XCl_4$ ($X=Cu, Cd, Mn, Fe$) lead to interesting behaviour in these compounds. The dielectric behaviour in the temperature ranges (10-300) K and (300-500) K, at frequencies between 100 Hz and 1 MHz are probed in $EA-CdCl_4$. Three structural transitions are observed around 475 K (T_{c1}), 214 K (T_{c2}) and 116 K (T_{c3}), in the heating cycle. The dielectric response with transition (T_{c2}) has been previously reported³¹. For a single crystalline c-plate, temperature dependent dielectric response in both heating and cooling run for temperature range 10 K to 300 K is shown in Fig 2.

Dielectric values decrease upon cooling and anomalies are seen at temperatures 212 K and 95 K both of which correspond to structural transitions (transition temperatures estimated by 1st order derivative of dielectric constant). A clear hysteresis is clearly observed in heating and cooling cycles at both transitions which indicate that the transition is first order in nature. The hysteresis width at T_{c3} transition is higher than that observed at T_{c2} , which is likely due to broad temperature region over which the transition at T_{c3} occurs. The magnitude of the dielectric constant observed parallel to the plane of crystal are much larger as compared to the values observed for in

3.1 Dielectric measurements

3 RESULTS AND DISCUSSIONS

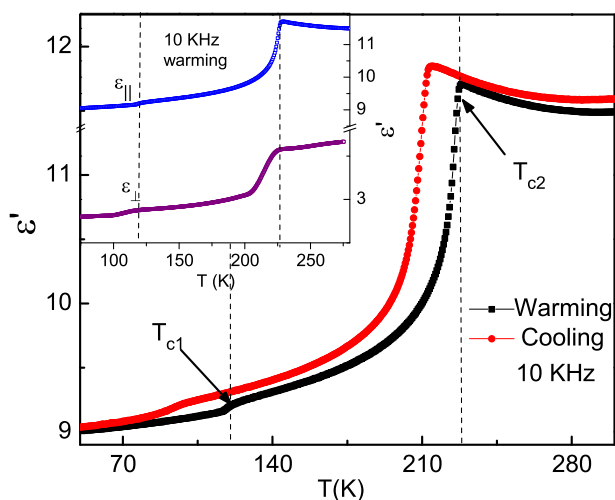


Figure 2 Temperature evolution of dielectric constant at 10 KHz frequency in both cooling and heating cycles. Inset shows temperature evolution of dielectric constants, both parallel and perpendicular to the crystal plate.

the plane perpendicular to the crystal as shown in the inset of Fig 2 (data collected during heating cycle). Though the transition resembles an antiferroelectric ordering and there is presence of low temperature anti-polar monoclinic phase, no antiferroelectric hysteresis loop is seen in PE loop measurements. The temperature at which the dielectric anomaly is observed does not shift with frequency but the magnitude of dielectric constant falls sharply as frequency increases. Temperature variation of dielectric parameters ϵ_1 (dielectric constant) and ϵ_2 (dielectric loss) in temperature range (320–500) K, is presented in Fig 3 and Fig 3-inset. The anomaly observed around 475 K (T_{c1}) is attributed to a structural phase transition. The high temperature transition in this compound has not been explored in detail so far, although similar transitions have been documented for EA-MnCl₄ and (CH₃NH₃)₂FeCl₄^{32,33} and assigned to the structural transition from tetragonal (*P4/mmm*) to orthorhombic phase. In many materials there is no dispersion is observed in the dielectric permittivity with frequency, across structural phase transition³⁴. However in many hybrid organic-inorganic compounds, dielectric relaxation/dispersion is observed across the transition due to reorientation of organic molecules^{32,35,36}. Such a relaxation process is characteristic of compounds with alkyl-ammonium ions³⁷. For the studied compound a small dispersion is observed across the structural transition as shown in Fig 3, which arises from the combined motion of (C₂H₅NH₃)⁺ cations.

To explore the relaxation process in EA-CdCl₄, we performed dielectric measurements in the range 100 Hz to 1 MHz at temperatures in the vicinity of the transition. The shape of curves fitted for imaginary part of dielectric constant (ϵ_2) as shown in

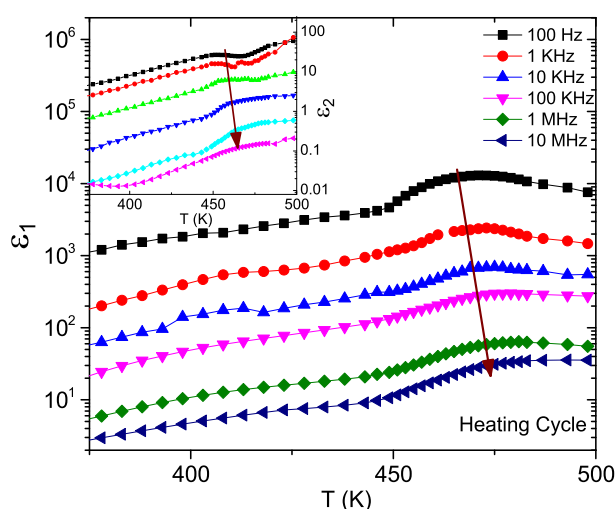


Figure 3 Temperature evolution of dielectric constant in temperature range (350 - 500) K for different frequency.

Fig 7 implies the existence of relaxation time distribution. The relaxation time distribution is then determined using Cole-Cole diagrams to elucidate the mechanism of relaxation.

$$\epsilon^* = \epsilon_1 + i\epsilon_2 \quad (1)$$

$$= \epsilon_\infty + (\epsilon_0 - \epsilon_\infty) / [1 + (i\omega\tau)^{1-\alpha}] \quad (2)$$

where, ϵ_0 and ϵ_∞ are static (low frequency) and high frequency dielectric constants, ω is angular frequency and τ is mean relaxation time. α is a parameter representing the distribution of relaxation times ($\alpha = 0$ for ideal Debye relaxation). The observed values of α were in the range 0.45 to 0.53 showing considerable change from ideal Debye like behavior. Equation 1 is separated into real and imaginary parts as below.

$$\epsilon_1 = \epsilon_\infty + ((\epsilon_0 - \epsilon_\infty)/2)[1 - \sinh\beta z / ((\cosh\beta z + \cos\beta\pi/2))] \quad (3)$$

and

$$\epsilon_2 = ((\epsilon_0 - \epsilon_\infty)/2)[\sinh\beta z / (\cosh\beta z + \cos\beta\pi/2)] \quad (4)$$

where, z is $\ln(\omega\tau)$ and β is $(1-\alpha)$. The frequency dependence of $\epsilon_2(T)$ is shown in Fig 4 for few select temperatures. For an inhomogeneous insulator, dielectric spectra has contributions from electrical conductivity. The above approximation allows to account for the contribution of electrical conductivity separately. The detailed analysis of ac conductivity shows exponential increase with temperature which is characteristic of hopping mechanism. An anomaly is observed near the transition temperature as shown in Fig 5(a).

The inset in Fig 5(a) ($\ln(\sigma)$ vs $1/T$) shows 2 linear segments and from the slope of these segments, we estimated activation

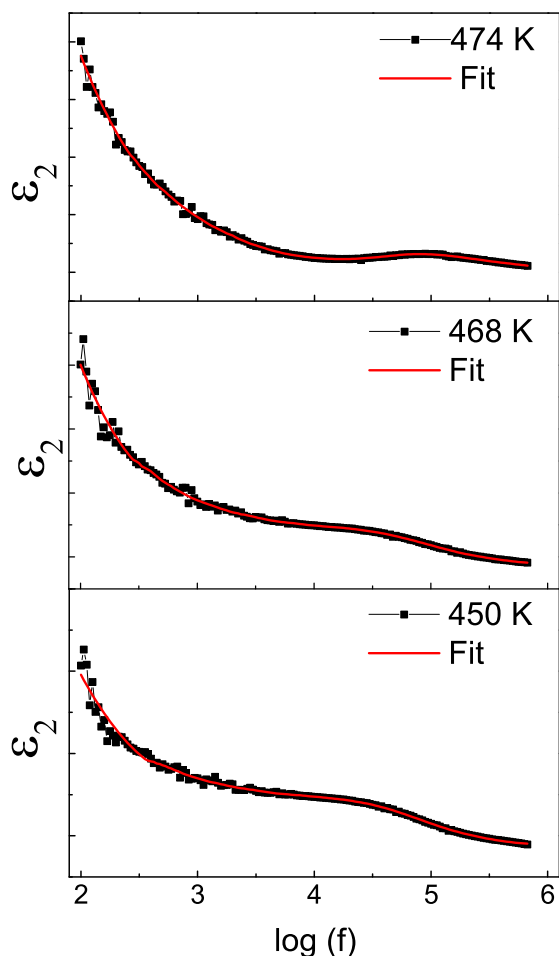


Figure 4 Frequency dependence of imaginary part of dielectric constant at various temperature.

energy for both phases. The values obtained for E_a is in the range 0.9 to 0.5 eV which are commensurate with the energy values for weak hydrogen bonds. This result confirms the proton character of the conductivity³⁸. Relaxation times are estimated by fitting the frequency dependent ϵ_2 at different temperatures, using equation 3. The values of relaxation time are observed in the range 10^{-3} - 10^{-6} s, characteristic of combined reorientation of ethyl-ammonium cations³⁹. Similar values are observed for the relaxation in EA-CuCl₄³². The temperature dependence of corresponding relaxation time is shown in Fig 5(b), which represents a linear behaviour in logarithmic scale (shown in inset of Fig 5(b)). The observed decrease in relaxation time with increase in temperature is related to the decrease in hydrogen bond strength.

Activation energy (E_r) for the relaxor behaviour can be calculated using Arrhenius equation.

$$\tau = \tau_0 \exp(E_r/kT) \quad (5)$$

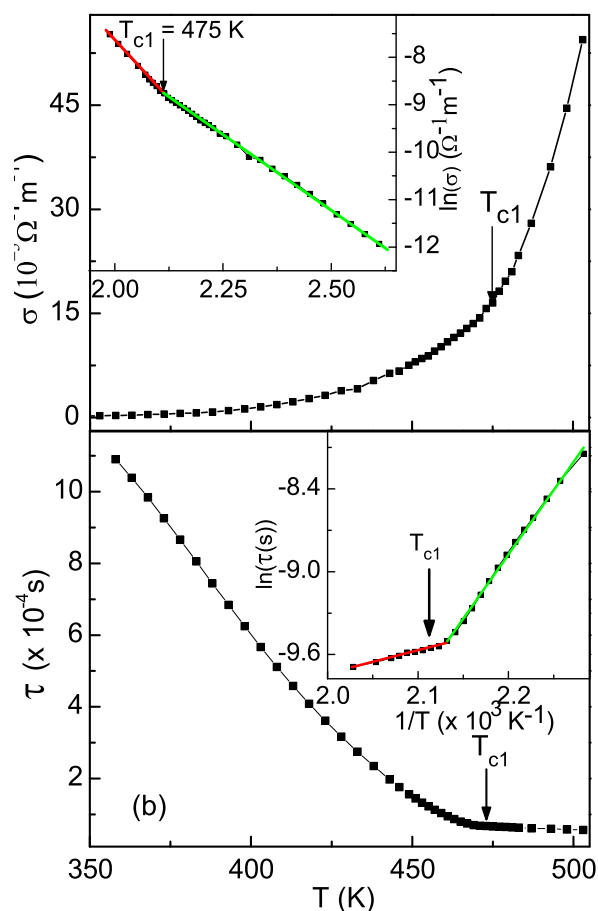


Figure 5 (a) Variation of ac conductivity with temperature. Inset shows $\ln(\sigma(1/T))$. (b) Variation of relaxation time with temperature. Inset shows $\ln(\tau(1/T))$.

The values of E_r obtained below the transition temperature is 0.715 eV, which is higher than the E_a value in the same region. The high temperature value of E_r is 0.124 eV which is small compared to E_a value in the same region. We have used impedance spectroscopy to study the multiple relaxations where different types of dielectric relaxations can be deconvoluted using an RC element model. For the ideal single relaxation $Z'-Z''$, the plot assumes the shape of a semicircle but considerable deviations are observed for real systems. In order to account for such non-ideal behaviour, the ideal capacitor is replaced with a constant phase element (CPE), with impedance defined as,

$$Z_{CPE}^* = 1/C_{CPE}(i\omega)^n \quad (6)$$

3.2 Raman Spectroscopy

3 RESULTS AND DISCUSSIONS

The impedance of the sample is measured at several temperatures and $Z'-Z''$ is plotted as shown in Fig 5. The data is fitted using 2 R-CPE units corresponding to contributions from bulk sample and the sample-electrode. The fitted curve for data corresponding to 450 K is shown in Fig 6 along with the equivalent circuit used for fitting. The fit parameters are $R_1 = 45439 \pm 1.281\%$, $R_2 = 66751 \pm 0.361\%$, $C_1 = 2.414 \text{ nF} \pm 1.365\%$, $n_1 = 0.74 \pm 0.142\%$, $C_2 = 0.499 \text{ pF} \pm 0.820\%$ and $n_2 = 0.884 \pm 0.06\%$. The high frequency response corresponds to the bulk contribution, while low frequency response is related to the sample-electrode interface.

It is known that the alkyl-ammonium cation complexes are dis-

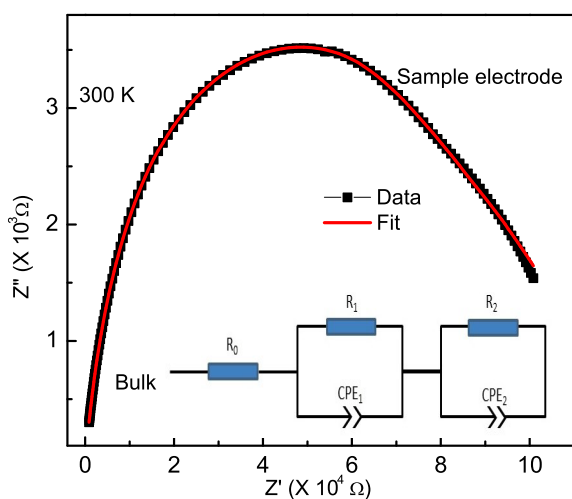


Figure 6 Experimental $Z'-Z''$ plot with a fit, for the observed data at 300 K. Inset shows the equivalent circuit used to the model the complex plane of impedance.

ordered at highest temperature¹⁵. NH_3 group of organic cations occupy cavities in metal halide octahedron and are linked to the metal halide complex by Hydrogen bonding. At highest temperature, the organic cations possess four equivalent states and they flip between these states. As the temperature decreases, the organic cation motion freezes stepwise from four to two and two to one at the corresponding transition temperatures (T_{c1} and T_{c2}). Low temperature monoclinic phase (at T_{c3}) is realized by non-linear coupling between organic cation and lattice. These results fairly co-relate with the lowering and dispersion in dielectric data obtained in the present study.

3.2 Raman Spectroscopy

The vibrational spectra of alkyl ammonium metal halide category of hybrid compounds can be divided in 2 regions. The region below 300 cm^{-1} describes external modes of crystal including vibrations of metal-halide octahedron, while the region above 300 cm^{-1} describes the internal vibrations of organic

cations. Although Raman spectra of EA- CdCl_4 is reported in the frequency range ($50 - 350 \text{ cm}^{-1}$) range by various groups^{21,23,40}, vibrational spectra for internal modes for organic ion have not been reported. R Kind et al have proposed a model of structural transition in $(\text{CH}_3\text{NH}_3)_2\text{CdCl}_4$, where phase transitions are described in terms of dynamic disorder of organic cations between four potential wells¹⁵. The change in orientation order of organic ion with temperature leads to structural transitions. This mandates a study of the internal vibrations of organic ions. In the present study, we have attempted to analyse the temperature dependent Raman Spectra for EA- CdCl_4 in the frequency range $150 - 4500 \text{ cm}^{-1}$ to understand the dynamics of structural phase transition. Fig 7 shows the spectra collected at room temperature, 220 K and 77 K which highlights significant changes in the modes observed at both temperatures. All the Raman active modes in the compound are assigned based on the calculation (using Guassian software) presented in Table 1 and are well supported by literature^{21,41}. The modes in various regions are divided into the following frequency classes: (i) Cd-Cl bending and stretching modes $150 - 300 \text{ cm}^{-1}$, (ii) C-N and C-H stretching modes $1000 - 1050 \text{ cm}^{-1}$, (iii) Symmetric and antisymmetric NH bending $1350 - 1800 \text{ cm}^{-1}$ and (iv) Symmetric and antisymmetric NH stretching $3000 - 3200 \text{ cm}^{-1}$. In addition, we also observed several modes arising due to N-H...Cl hydrogen bond, torsional motion of molecular subunits and combination modes and overtone of C-N and C-H vibrations.

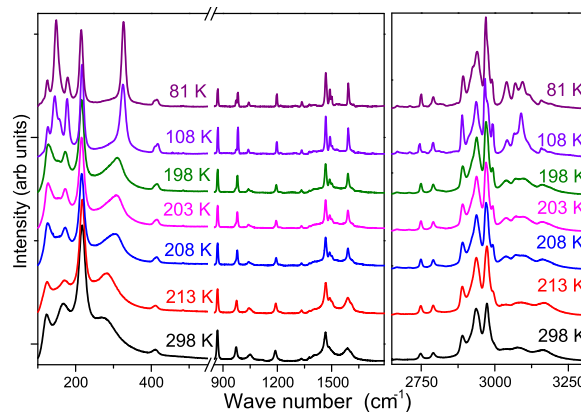


Figure 7 Raman spectra of $(\text{C}_2\text{H}_5\text{NH}_3)_2\text{CdCl}_4$ at 77 K and 300 K in the frequency range ($150 - 4500 \text{ cm}^{-1}$).

Near the phase transition temperatures, significant spectral changes are observed. The transitions are in agreement with the transition temperatures reported in single crystal X ray diffraction study¹⁴ and dielectric measurements reported in the present work. We used the temperature evolution of vibrational frequencies and full width at half maximum (FWHM) related to vibrations/bending modes of various molecular subunits to

3.2 Raman Spectroscopy

3 RESULTS AND DISCUSSIONS

Table 1 Calculated vibrational wave-numbers, observed Raman band positions and assignment for $(C_2H_5NH_3)_2CdCl_4$.

Calculated	Experimental	Mode Assignment
191	176	δ (Cd–Cl)
206	216	ν (Cd–Cl)
268	275	τ (NH ₃)
384	409	ρ (NH ₃)
805	798	ρ (NH ₃)
865	870	ν (C–N)
963	971	ρ (NH ₃)
1005	1047	δ (C–C–N) bend
1177	1186	δ_s (NH ₃)
1212	1216	δ_s (NH ₃), δ_s (NH ₃)
1314	1333	δ (NH ₃), δ (CH ₂)
1370	1375	δ (CH ₂) (umbrella reformation)
1461	1465	δ (CH ₂) (scissoring), δ_a (CH ₃)
1631	1613	δ (N–H) (bend), δ (NH ₃)
2945	2891	ν_s (CH ₃)
2982	2939	ν (N–H), ν_s (CH ₂)
2989	2972	ν (N–H), ν_s (CH ₂)
3003	2990	ν (N–H)
3050	3039	ν (N–H)
3130	3070	ν (N–H ₂)
3169	3098	ν_a (N–H)
3264	3158	ν_a (N–H)

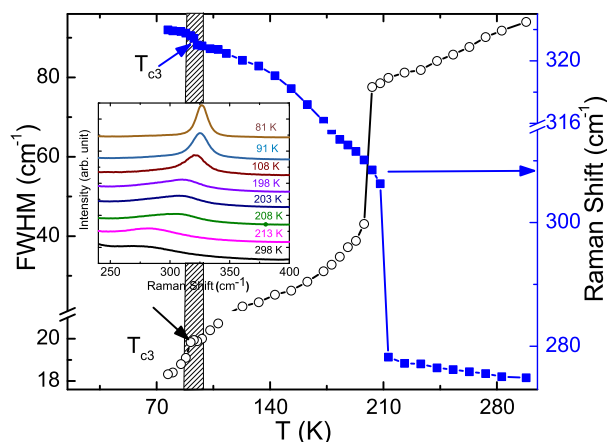
ν stretching; δ deformation; ρ rocking; τ torsion

explain the dynamics driving these phase transitions. At room temperature, EA- $CdCl_4$ is in $Bmab$ orthorhombic phase and the ethyl-ammonium ions are disordered with two symmetrically equivalent orientations as shown by the X-Ray diffraction studies¹⁴. Below the phase transition (216 K) only one orientation remains and the system transforms to $Pbca$ space group. The spectral features below 300 cm^{-1} , matches well with earlier investigations. The frequency of internal vibrations of $C_2H_5NH_3^+$ molecular group generally lie above 300 cm^{-1} , so molecular group can be considered rigid with only translational and rotational (libration) degrees of freedom. Three frequencies centred at 122, 170, and 216 are observed in the spectral region below 300 cm^{-1} as shown in Supplementary data (Fig S1). One more mode is observed at 275 cm^{-1} , which is shown in Fig 8.

The peak close to 120 cm^{-1} is assigned to the translatory and rotatory modes of the ethyl ammonium group, while the one at 216 cm^{-1} is consequent to symmetrical stretching of Cd–Cl octahedron due to vibrations of Cd and Cl atoms at axial positions²¹. The frequency mode observed at 170 cm^{-1} arises from displacements of axial and equatorial chlorine atoms which cause Cd-Cl bending²¹. A broad feature is observed at 275 cm^{-1} which is assigned to internal torsional motion of NH₃ in the organic group⁴⁰. It is worth noting that in isolated $CH_3NH_3^+$ group, NH₃ torsion motion is neither Raman nor IR active. So even in $C_2H_5NH_3^+$, it is supposed to be inactive. The presence

of torsional mode is attributed to the intramolecular interactions of NH₃ with chlorine atoms through N–H \cdots Cl hydrogen bonds. This band shifts to higher frequency below T_{c2} , as shown in Fig 8. Upon cooling from room temperature to 77 K, we observe abrupt changes for frequencies 168 and 275 cm^{-1} near T_{c2} , while minute changes are seen in the vicinity of $T_{c3} = 114\text{ K}$. The abrupt shift to higher frequency in the torsional mode of NH₃ on cooling is consistent with hydrogen bond strengthening at low temperature, due to ordering of organic ion chain.

In the range, $500 - 1750\text{ cm}^{-1}$, several deformation and

**Figure 8** Temperature evolution of raman shift and fwhm of torsional mode of NH₃. Inset shows temperature evolution of NH₃ torsion mode.

C–N, C–H stretching modes are observed, as seen in Table 1. The temperature evolution of these modes are shown in Supplementary data Fig S2 and S3. Many of these modes, undergo marked change across T_{c2} , while negligible or no change is observed across T_{c3} . FWHM of few deformation modes of NH₃ show small change across T_{c3} as shown in Fig 9(a).

The stretching modes of ammonium end of alkyl ammonium ion are presented in Fig 9(b) and (c). Stretching modes of X–H (X = O, N...) seen in the high frequency region above 2000 cm^{-1} and do not interact with other vibrations except X–H stretches. X–H bonds can easily form hydrogen bonding X–H \cdots , which drastically lowers the stretching frequency but are identified from broadening and intensification of bands/modes. Although hydrogen bond has a weak interaction, it produces significant changes in the vibrational spectra. In EA- $CdCl_4$, hydrogen bond with chlorine (Cl), resulting in lowering of N–H and C–H stretching modes.

C–H symmetric and antisymmetric stretching modes typically occur in the range $2800\text{ to }3000\text{ cm}^{-1}$. One Symmetric (2889 cm^{-1}) and two antisymmetric stretching modes at 2972 and 2982 cm^{-1} are seen in this range, for $-CH_3$ group. The asymmetric peak at 2972 cm^{-1} softens with temperature

and abruptly shift to 2968 cm^{-1} at T_{c2} and splits to give one more mode at 2974 cm^{-1} . The CH_2 group associated with N, also gives rise to C–H antisymmetric stretching mode at 2923 cm^{-1} , which splits to give rise to another peak while approaching T_{c3} . Due to vibrational coupling between identical C–H vibrational modes sharing the same C atom, 3 additional frequencies are evident: one symmetric and 2 anti-symmetric. The former occurs at low frequency, while antisymmetric mode occurs at higher frequency. There is no coupling between C–H modes belonging to different C atoms. Similarly, N–H symmetric and antisymmetric stretching modes are observed in the range 2900 to 3200 cm^{-1} . N–H stretching generally correspond to 3400 cm^{-1} but the frequency reduces sharply in case of hydrogen bonding. In $(\text{C}_2\text{H}_5\text{NH}_3)_2\text{CdCl}_4$, N–H forms hydrogen bond with Cl atom of Cd–Cl octahedron which lowers the frequency of N–H stretching modes resulting in modes at 2990 cm^{-1} (symmetric); 3073 and 3098 cm^{-1} (antisymmetric). Other modes are seen at 3035 and 3185 cm^{-1} due to coupling between identical N–H stretching. All modes in this region soften with decrease in temperature and anomalies are seen at both T_{c2} and T_{c3} .

Raman studies show significant changes in the temperature de-

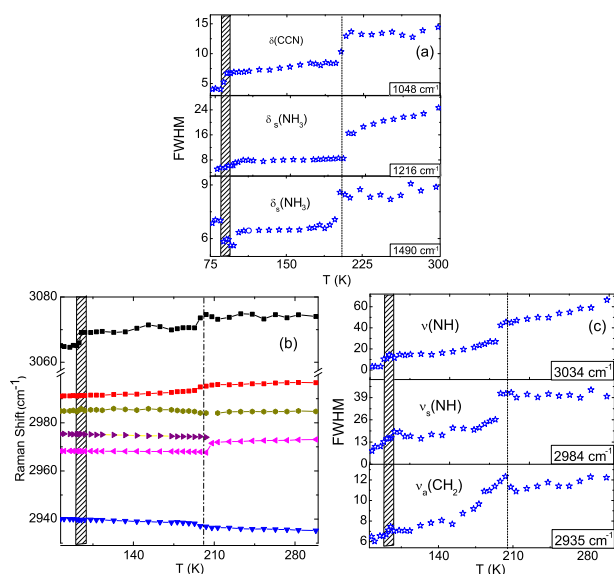


Figure 9 (a) Temperature evolution of Fwhm of various NH_3 deformation modes in the temperature range $77 - 298\text{ K}$. (b) Temperature evolution of Raman shift of symmetric and antisymmetric stretching modes of N–H and C–H bonds $(\text{C}_2\text{H}_5\text{NH}_3)_2\text{CdCl}_4$. (c) Temperature evolution of Fwhm of corresponding vibrational modes in the temperature range $77 - 298\text{ K}$.

pendence of the wavenumber and fwhm of various vibrational modes in the proximity of the structural transitions observed below room temperature. The temperature dependence of in-

ternal modes and its fwhm of organic cations consolidates their (reorientation order) role in structural modifications. The observed results are consistent with the theoretical predications for $(\text{CH}_3\text{NH}_3)_2\text{CdCl}_4$. From the structural data available, it is known that at room temperature, the system is disordered and the C–C bond is constrained to lie on a mirror plane yielding two equivalent positions for the organic chain. Hence, the symmetry equivalent chains influence the Cd–Cl octahedron via hydrogen bonding leading to an anomaly in bending mode for the octahedron across T_{c2} . The number of symmetrically equivalent sites reduces resulting in structural transition at T_{c2} which is reflected in the vibrational modes associated with both Cd–Cl octahedron and external and internal vibrations of the organic chain. The monoclinic transition can't be explained in terms of order-disorder model. Further it can be explained in terms of non-linear coupling of organic chain motion with the Cd–Cl octahedron. Since, the Cd–Cl octahedron is weakly coupled with the organic chain through hydrogen bonding, the changes in vibrational spectra at T_{c3} are not as prominent as that at T_{c2} . Very few modes associated with C–N and N–H stretching modes show small variation across T_{c3} . Despite lack of single crystal data to confirm the existence of monoclinic phase at low temperature, theoretical calculations and Raman studies on $(\text{CH}_3\text{NH}_3)_2\text{CdCl}_4$ predict a monoclinic phase with space group $P2_1/b$. $(\text{C}_2\text{H}_5\text{NH}_3)_2\text{CdCl}_4$ also belongs to the same family of compounds and a similar monoclinic structure has been predicted. It is worth noting that $P2_1/b$ space is a maximal subgroup of $Pbca$ space group and does not satisfy Landau condition⁴² for a second-order transition according to Geick and Strobel criterion⁴³. This implies towards presence of first order transition which has been seen in the heating and cooling cycles of dielectric measurements. However, the observed raman behaviour of few NH_3 vibration mode across T_{c3} point out to a first order-like transition, instead of strongly first order nature and occurs over a broad range of temperature. On the basis of linewidth as function of temperature, it can be asserted that this transition is related to torsion and libration motions of organic group and is associated with a small distortion of lattice. The transition is displacive in nature, rather than an order-disorder transition and is therefore very weak in nature, manifested only in few raman modes belonging to motion of organic group. On the basis of dielectric and Raman studies, we postulate 4 phases of $(\text{C}_2\text{H}_5\text{NH}_3)_2\text{CdCl}_4$ evolving with temperature. The system consolidates into a tetragonal $I4/mmm$ phase at high temperature. As the material is cooled, it undergoes structural transition to orthorhombic $Bmab$ phase, which later transforms to $Pcab$ phase at about 214 K . Further an addition structural transition is observed below 110 K where the system goes to monoclinic symmetry.

REFERENCES

REFERENCES

4 Conclusion

The dynamics of phase transitions in $(\text{C}_2\text{H}_5\text{NH}_3)_2\text{CdCl}_4$ are understood by dielectric and Raman studies. The anomalies observed in vibrational frequencies and fwhm at transition temperature are attributed to phase transitions. Dielectric measurements regard these anomalies in the perspective of three transition temperatures. The phase transitions are driven by the ordering of $(\text{C}_2\text{H}_5\text{NH}_3)^+$ ion. Internal vibrations of N–H and C–N stretching modes and their FWHM provide additional insight to the ordering mechanism for low temperature transitions. High temperature dielectric response describe relaxation behaviour and are believed to be considerably different from ideal Debye type relaxation. The dielectric constant increases with temperature while relaxation time decreases for high temperature phase. The observed decrease in relaxation time can be correlated with weakening of H-bonds as the temperature increases. The determined relaxation time is characteristic of the combined reorientation of ethyl-ammonium groups. Raman and dielectric studies confirm the existence of all 4 phases in $(\text{C}_2\text{H}_5\text{NH}_3)_2\text{CdCl}_4$.

5 Acknowledgement

Ruchika Yadav and Partha P. Kundu wishes to acknowledge Council for Scientific and Industrial Research, India for fellowship. Thanks are due to Department of Science and Technology, India for financial support through project grant.

References

- [1] A. K. Cheetham and C. N. R. Rao, *Science*, 2007, **318**, 58–9.
- [2] A. H. Arkenbout, T. Uemura, J. Takeya and T. T. M. Palstra, *Appl. Phys. Lett.*, 2009, **95**, 173104.
- [3] S. Kitagawa, R. Kitaura and S.-i. Noro, *Angew. Chem. Int. Ed. Engl.*, 2004, **43**, 2334–75.
- [4] C. N. R. Rao, A. K. Cheetham and A. Thirumurugan, *J. Phys. Condens. Matter*, 2008, **20**, 083202.
- [5] O. M. Yaghi, G. Li and H. Li, *Nature*, 1995, **378**, 703–706.
- [6] A. K. Cheetham, C. N. R. Rao and R. K. Feller, *Chem. Commun.*, 2006, 4780.
- [7] D. B. Mitzi, *J. Chem. Soc. Dalton Trans.*, 2001, **48**, 1–12.
- [8] D.-f. Weng, Z.-m. Wang and S. Gao, *Chem. Soc. Rev.*, 2011, **40**, 3157–81.
- [9] M. Kurmoo, *Chem. Soc. Rev.*, 2009, **38**, 1353–79.
- [10] W. Zhang and R.-g. Xiong, *Chem. Rev.*, 2012, **112**, 1163–95.
- [11] P. Jain, V. Ramachandran, R. J. Clark, H. D. Zhou, B. H. Toby, N. S. Dalal, H. W. Kroto and A. K. Cheetham, *J. Am. Chem. Soc.*, 2009, **131**, 13625–7.
- [12] M. Sánchez-Andújar, S. Presedo, S. Yáñez Vilar, S. Castro-García, J. Shamir and M. A. Señarís Rodríguez, *Inorg. Chem.*, 2010, **49**, 1510–6.
- [13] G.-c. Xu, W. Zhang, X.-M. Ma, Y.-h. Chen, L. Zhang, H.-l. Cai, Z.-m. Wang, R.-g. Xiong and S. Gao, *J. Am. Chem. Soc.*, 2011, **133**, 14948–51.
- [14] G. Chapuis, *Phys. Status Solidi*, 1977, **43**, 203–212.
- [15] R. Kind, R. Blinc and B. Žekš, *Phys. Rev. B*, 1979, **19**, 3743–3754.
- [16] J. Steadman and R. Willett, *Inorganica Chim. Acta*, 1970, **4**, 367–371.
- [17] B. Kundys, A. Lappas, M. Viret, V. Kapustianyk, V. Rudyk, S. Semak, C. Simon and I. Bakaimi, *Phys. Rev. B*, 2010, **81**, 224434.
- [18] Y. Takehisa, *J. Phys. Soc. Jpn.*, 1989, **58**, 2276.
- [19] K. Ohwada, K. Ishii, T. Inami, Y. Murakami, T. Shobu, H. Ohsumi, N. Ikeda and Y. Ohishi, *Phys. Rev. B*, 2005, **72**, 014123.
- [20] V. Kapustianyk, V. Rudyk and M. Partyka, *Phys. status solidi*, 2007, **244**, 2151–2158.
- [21] H. Hagemann and H. Bill, *J. Phys. C Solid State Phys.*, 1985, **18**, 6441–6456.
- [22] R. Kind, *Ferroelectrics*, 1980, **24**, 81–88.
- [23] H. Hagemann and H. Bill, *Chem. Phys. Lett.*, 1982, **87**, 45–49.
- [24] M. Couzi, A. Daoud and R. Perret, *Phys. Status Solidi*, 1977, **41**, 271–282.
- [25] G. V. P. Kumar and C. Narayana, *Curr. Sci.*, 2007, **93**, 778–791.
- [26] M. Frisch, G. Trucks, H. Schlegel, G. Scuseria, M. Robb, J. Cheeseman, V. Zakrzewski, J. Montgomery Jr, R. Stratmann, J. Burant *et al.*, *GAUSSIAN software*, 2003.
- [27] A. D. Becke, *J. Chem. Phys.*, 1993, **98**, 5648.
- [28] C. Lee, C. Hill and N. Carolina, 1988, **37**, year.

REFERENCES

REFERENCES

- [29] P. J. Hay and W. R. Wadt, *J. Chem. Phys.*, 1985, **82**, 270.
- [30] R. D. Johnson III, *Johnson III* <http://srdata.nist.gov/cccbdb>, 2005.
- [31] A. Levstik and C. Filipič, *Phys. Status Solidi*, 1980, **58**, K165–K166.
- [32] Y. Korchak, V. Kapustianik, R. Tchukvinskyi, Z. Czapla, S. Dacko and V. Bazhan, *Phys. status solidi*, 2001, **228**, 777–784.
- [33] J. Han, S. Nishihara, K. Inoue and M. Kurmoo, *Inorg. Chem.*, 2014, **53**, 2068–75.
- [34] D. Zhou, W.-B. Li, L.-X. Pang, Z.-X. Yue, G.-S. Pang and X. Yao, *RSC Advances*, 2015, **5**, 19255–19258.
- [35] B. Pato-Doldán, M. Sánchez-Andújar, L. Gómez-Aguirre, S. Yáñez-Vilar, J. López-Beceiro, C. Gracia-Fernández, A. Haghighirad, F. Ritter, S. Castro-García and M. Señarís-Rodríguez, *Physical Chemistry Chemical Physics*, 2012, **14**, 8498–8501.
- [36] T. Besara, P. Jain, N. S. Dalal, P. L. Kuhns, A. P. Reyes, H. W. Kroto and A. K. Cheetham, *Proceedings of the National Academy of Sciences*, 2011, **108**, 6828–6832.
- [37] V. B. Kapustianik, H. Kabelka, H. Warhanek and A. Fuith, *Phys. Status Solidi*, 1996, **155**, 95–113.
- [38] V. Kapustianik, I. Polovinko, Y. Korchak, S. Sveleba, R. Tchukvinskyi and S. Kaluza, *Phys. status solidi*, 1997, **161**, 515–521.
- [39] I. R. Jahn, K. Schwab, K. Knorr and K. Holocher, *J. Phys. Condens. Matter*, 1994, **6**, 10839–10853.
- [40] R. Mokhlisse, *J. Chem. Phys.*, 1982, **77**, 1138.
- [41] D. W. Mayo, F. A. Miller and R. W. Hannah, *Course Notes on the Interpretation of Infrared and Raman Spectra*, John Wiley & Sons, Inc., Hoboken, NJ, USA, 2004.
- [42] A. Bruce and R. A. Cowley, *Structural phase transitions*, Taylor and Francis, 1981, vol. 29.
- [43] R. Geick and K. Strobel, *Journal of Physics C: Solid State Physics*, 1977, **10**, 4221.